

# A systematic study on the cosmic ray antiproton flux

Su-Jie Lin<sup>1</sup>, Xiao-Jun Bi<sup>1</sup>, Jie Feng<sup>2</sup>, Peng-Fei Yin<sup>1</sup>, Zhao-Huan Yu<sup>1,3</sup>

<sup>1</sup>*Key Laboratory of Particle Astrophysics, Institute of High Energy Physics,  
Chinese Academy of Sciences, Beijing 100049, China*

<sup>2</sup>*School of Physics and Engineering, Sun Yat-Sen University,  
Guangzhou 510275, P. R. China and*

<sup>3</sup>*ARC Centre of Excellence for Particle Physics at the Terascale,  
School of Physics, The University of Melbourne, Victoria 3010, Australia*

## Abstract

Recently the AMS-02 collaboration has published the measurement of the cosmic antiproton to proton ratio  $\bar{p}/p$  and the  $\bar{p}$  flux with a high precision up to  $\sim 450$  GeV. In this work, we perform a systematic analysis of the secondary antiproton flux generated by the cosmic ray interaction with the interstellar gas. The uncertainty of the prediction originates from the cosmic ray propagation process and the hadronic interaction models. Although the cosmic ray propagation parameters have been well controlled by the AMS-02  $B/C$  ratio data for a specified model, different propagation models can not be discriminated by the  $B/C$  data. The  $\bar{p}$  flux is also calculated for several hadronic interaction models, which are generally adopted by the cosmic ray community. However, the results for different hadronic models do not converge. We find the EPOS LHC model, which seems to fit the collider data very well, predicts a slightly lower  $\bar{p}/p$  ratio than the AMS-02 data at the high energy end. Finally we derive the constraints on the dark matter annihilation cross section from the AMS-02  $\bar{p}/p$  ratio for different propagation and hadronic interaction models.

PACS numbers: 96.50.S-,95.35.+d

## I. INTRODUCTION

Antimatter searches in cosmic rays (CRs) are especially important for astrophysics and dark matter (DM) indirect detection. In recent years, there were great progresses in the measurements of CR antimatter particles. In particular, the Alpha Magnetic Spectrometer (AMS-02) launched in 2011 has provided unprecedentedly precise CR measurements. Based on the results from AMS-02 [1] and previous experiments, such as PAMELA [2] and Fermi-LAT[3], the properties of CR antimatter particles have been extensively studied in a quantitative way in the literature.

Recently, the AMS-02 collaboration has published the measurements of the  $\bar{p}/p$  ratio and the  $\bar{p}$  flux up to  $\sim 450$  GeV with a high precision [4]. The major challenge to interpret the AMS-02 data and search for potential DM signals is how to predict the secondary antiproton flux precisely. The secondary antiprotons are generated by collision between the high energy cosmic rays and the interstellar gas. Its flux is determined by the CR propagation process and its hadronic interaction with the interstellar gas, both of which have relatively large uncertainties at present. In this work, we perform a systematic analysis of the secondary antiproton flux considering these possible uncertainties carefully. Some relevant discussions can also be found in Refs. [5–14]

The CR propagation in the Galaxy involves many complicated effects, such as the diffusion, energy loss, convection, and reacceleration. The propagation parameters describing these effects can be determined by fitting to the secondary-to-primary nuclei ratios, such as B/C and (Sc+Ti+V)/Fe, and unstable-to-stable ratios of secondary nuclei, such as  $^{10}\text{Be}/^9\text{Be}$  and  $^{26}\text{Al}/^{27}\text{Al}$  [15–18], where the secondary nuclei are generated by the primary nucleus collision with the interstellar matter when they are propagating. However, the current measurements of these ratios remain not sufficient to distinguish different propagation models. Therefore the propagation is one of the main sources of uncertainty when predicting the secondary antiproton flux. Another important uncertainty of propagation comes from the solar modulation [19]. This effect significantly affects low energy CR spectra, but is difficult to precisely quantify.

In this work, the GALPROP package is used to solve the CR propagation equation [15, 20]. We adopt three kinds of propagation models, namely the diffusion-reacceleration (DR) model, the modified diffusion-reacceleration (DR-2) model, and the diffusion-convection

(DC) model. Propagation parameters are determined by fitting the available B/C data with a Markov Chain Monte Carlo (MCMC, [21]) algorithm [22–25], which is powerful for surveying high dimensional parameter space.

The hadronic interaction between CR particles and interstellar gas is another important source of uncertainty for calculating the antiproton flux. Although Quantum Chromodynamics (QCD) is well-established as the theory of strong interaction and has been confirmed at collider experiments, only the processes with large momentum transfers can be predicted by the perturbative calculation from the first principle. It is not possible to calculate the forward scattering processes with multiparticle production by QCD, such as the CR interaction with interstellar gas considered here. In order to calculate such hadronic processes, some simplified assumptions and phenomenological/empirical parametrization are needed.

In the cosmic ray study, it has been a long time difficulty to deal with the hadronic interaction. Many phenomenological forms have been proposed in the literature to describe the hadronic interaction. Unfortunately, there is no consensus on the empirical hadronic model so far. In this work, we discuss the impact of hadronic models on the antiproton production. We find that the hadronic interaction induces the largest uncertainty in the prediction of the antiproton flux.

Based on the predicted  $\bar{p}$  flux and the AMS-02 measurement, we derive constraints on the DM annihilation cross section in different hadronic interaction and CR propagation models.

This paper is organized as follows. In Sec. II, we describe the CR propagation processes. In Sec. III, we introduce the hadronic interaction models and compare the prediction with accelerator data. The secondary antiproton flux and  $\bar{p}/p$  ratio prediction are presented in Sec. IV. In Sec. V, we investigate the implications for DM annihilation from the AMS-02  $\bar{p}/p$  measurement and the CRs prediction. Finally, we give the summary and discussions in Sec. V.

## II. PROPAGATION OF GALACTIC COSMIC RAYS

After accelerated in sources, Galactic CRs are injected and diffuse in the interstellar space and suffer from several propagation effects before arriving at the Earth. A conventional assumption is that CRs propagate in a cylindrical halo with a half height  $z_h$ , beyond which

CRs escape freely. The propagation equation can be expressed as [26]

$$\begin{aligned} \frac{\partial \psi}{\partial t} = & Q(\mathbf{x}, p) + \nabla \cdot (D_{xx} \nabla \psi - \mathbf{V}_c \psi) + \frac{\partial}{\partial p} \left[ p^2 D_{pp} \frac{\partial}{\partial p} \left( \frac{\psi}{p^2} \right) \right] \\ & - \frac{\partial}{\partial p} \left[ \dot{p} \psi - \frac{p}{3} (\nabla \cdot \mathbf{V}_c) \psi \right] - \frac{\psi}{\tau_f} - \frac{\psi}{\tau_r}, \end{aligned} \quad (1)$$

where  $Q(\mathbf{x}, p)$  is the CR source term,  $\psi = \psi(\mathbf{x}, p, t)$  is the CR density per momentum interval,  $\dot{p} \equiv dp/dt$  is the momentum loss rate, and the time scales  $\tau_f$  and  $\tau_r$  characterize fragmentation processes and radioactive decays, respectively.

It is generally believed that CR particles are accelerated in supernova remnants (SNRs). Thus the spatial distribution of the CR sources follows the SNR distribution as

$$f(r, z) = \left( \frac{r}{r_\odot} \right)^a \exp \left[ -\frac{b(r - r_\odot)}{r_\odot} \right] \exp \left( -\frac{|z|}{z_s} \right), \quad (2)$$

where  $r_\odot = 8.5$  kpc is the distance from the Sun to the Galactic Center, and  $z_s \simeq 0.2$  kpc is the characteristic height of the Galactic disk. We adopt  $a = 1.25$  and  $b = 3.56$  [27] in the calculation. The injection spectra are assumed to be broken power-law functions with respect to the rigidity.

The spatial diffusion coefficient  $D_{xx}$  can be parametrized as [28]

$$D_{xx} = D_0 \beta^\eta (R/R_0)^\delta, \quad (3)$$

where  $R \equiv pc/Ze$  is the rigidity,  $\beta$  is the CR particle velocity in units of the light speed  $c$ ,  $R_0$  is the reference rigidity and  $D_0$  is a normalization parameter. Although the slop of diffusion coefficient  $\delta$  is predicted to be  $\delta = 1/3$  for a Kolmogorov spectrum of interstellar turbulence, or  $\delta = 1/2$  for a Kraichnan cascade, this parameter is usually treated as a free parameter when explaining data. The factor of  $\beta^\eta$  denotes the effect that the diffusion coefficient could be altered at low velocities due to the turbulence dissipation. We take  $\eta = 1$  as the standard diffusion plus reacceleration (DR) case taken in GALPROP. We refer the case with  $\eta = -0.4$  as the DR-2 model, which can improve the secondary fitting as discussed in [29].

The CR reacceleration process due to collisions on interstellar random weak hydrodynamic waves can be described by the diffusion in momentum space with a coefficient  $D_{pp}$ , which is related with  $D_{xx}$  by [30]

$$D_{pp} D_{xx} = \frac{4p^2 v_A^2}{3\delta(4 - \delta^2)(4 - \delta)\omega}, \quad (4)$$

where  $v_A$  is the Alfvén velocity and  $\omega$  is the ratio of the magnetohydrodynamic wave energy density to the magnetic field energy density. Since  $D_{pp}$  is proportional to  $v_A^2/\omega$ , we can set  $\omega = 1$  and just use  $v_A$  to characterize the reacceleration effect. The convection velocity  $\mathbf{V}_c$  is usually assumed to linearly depend on the distance away from the Galactic disk and the convection effect can be described by the quantity  $dV_c/dz$ . Therefore, the major propagation parameters involve  $D_0$ ,  $\delta$ ,  $R_0$ ,  $\eta$ ,  $v_A$ ,  $dV_c/dz$ , and  $z_h$ .

When CRs propagate in the solar system, their spectra with  $R \lesssim 20$  GV are significantly affected by solar winds. This is the solar modulation effect, which depends on solar activities and varies with the solar cycle. It can be described by the force field approximation [19] with only one parameter, i.e., the solar modulation potential  $\phi$ .

Due to fragmentation and radioactive decays, secondary CR particles are produced in propagation processes. As a result, secondary-to-primary ratios and unstable-to-stable secondary ratios, such as B/C and  $^{10}\text{Be}/^9\text{Be}$ , are sensitive to propagation parameters, but almost independent of primary injection spectra. Thus the measurements of these ratios are useful for determining the propagation parameters (see e.g. Refs. [27, 31]).

Note that there are degeneracies between the propagation models with the reacceleration process and those with the convection effect. Current measurements are not sufficient to distinguish these models. Therefore, we separately consider the DR, DR-2, and DC models when calculating the antiproton flux.  $R_0$  is taken to be 4 GV in the DR and DR-2 models. In the DC model, however,  $R_0$  is set to be a free parameter and  $\delta = 0$  is imposed for  $R < R_0$ .

### III. HADRONIC INTERACTION MODELS

Although QCD has been proved to be a very successful theory of the strong interaction, we do not have a realistic technique to calculate the bulk of multiparticle production in hadronic interactions from the first principle. Many phenomenological and empirical models have been developed to explain the collider and cosmic ray data. These models include a large number of parameters that encode the fundamental physics and phenomenological descriptions of the fragmentation process.

These hadronic models could be classified into three categories according to their purposes. HERWIG[32], PYTHIA[33] and SHERPA[34] are generally adopted in high energy physics (HEP) studies, and focus on hard-scattering processes at accelerator experiments.

In contrast, QGSJET01[35], QGSJET II[36, 37] and SIBYLL[38–40] are designed for simulating the extensive air showers caused by the high energy CR particles. Therefore, these models focus on the bulk production of soft particles with low transverse momenta, and emphasize on providing a reasonable extrapolation for higher energy and wider phase-space regions. PHOJET[41–43], DPMJET[44] and EPOS[45, 46] fall in between these two categories. These models can also approach the HEP models regarding the hard process, and are adjusted to well reproduce the low energy accelerator data.

The HEP models listed above are not considered in our calculation, as they are not suitable for dealing with CRs interaction with the interstellar gas. As the hadronic models proposed for the CR interaction mainly focus on the high energy region, the description of the interaction for CRs below 100 GeV may be not precise. Fortunately, in recent years many new data sets measured at LHC and fixed-target experiments are available. New versions of QGSJET II-04 [47] and EPOS LHC[46] have been released whose model parameters are tuned to fit these data [48–52]. The EPOS LHC model fits the available accelerator antiproton data in all energy regions. Recently the QGSJET II-04 has been slightly modified to better reproduce the accelerator antiproton data at low energies, referred to as QGSJET II-04m here [53]. In the following, we use EPOS LHC and QGSJET II-04m to calculate the CR antiproton flux. Another version of EPOS, namely EPOS 1.99[54], is also considered in the calculation, since this version has been more carefully tuned to fit the low energy accelerator data, such as the measurements of NA49 and NA61[55].

For comparison, we also consider the default hadronic model embedded in GALPROP [56], which is referred to as Tan & Ng + BP01. In this model, a parametrization given by Tan & Ng [57] and a code from Barashenkov & Polanski are combined to estimate the  $\bar{p}$  spectrum. Other models for high energy air showers (QGSJET01, QGSJETII and SIBYLL) are not used to predict the CR antiproton flux, as they do not aim at describing the low energy CR interactions considered here.

In the following we compare the expectations of different hadronic models with the accelerator measurements of the process  $pp \rightarrow \bar{p}X$ . In Figs. 1 and 2 we show the cross section of  $pp \rightarrow \bar{p} + X$  as a function of  $x_F \equiv 2p_z/\sqrt{s}$  in the center-of-mass system for specified transverse momentum  $p_T$  and integrated cross section over  $p_T$  for different hadronic models respectively. The expectation is compared with the NA49 data [58, 60], which is a fixed target experiment with the incoming beam momentum of 158GeV/ $c$ . In Fig. 1, we consider

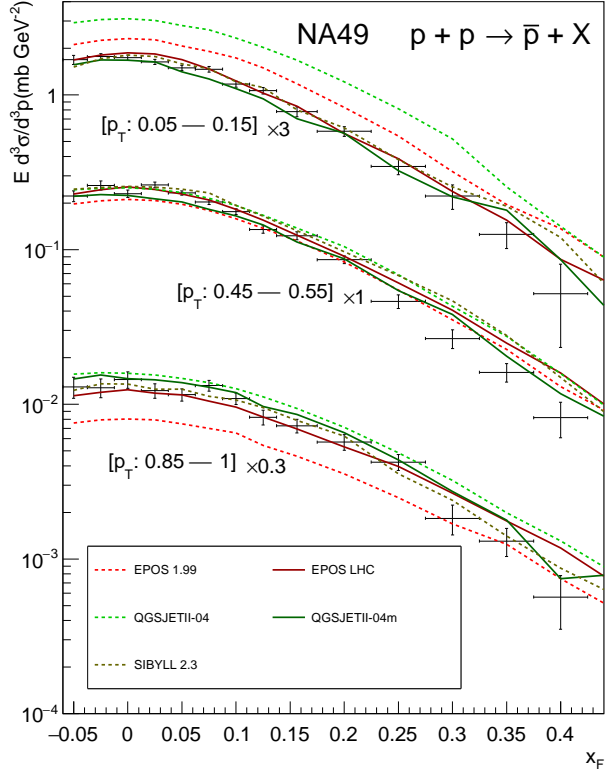


FIG. 1. The differential cross section of  $E d^3 \sigma / d^3 p$  for the  $p + p \rightarrow \bar{p} + X$  process compared with the NA49 measurement [58], with variables given in the center-of-mass system. Three groups of curves from the top to bottom correspond to the  $p_T$  ranges of  $[0.05 - 0.15]$  GeV,  $[0.45 - 0.55]$  GeV and  $[0.85 - 1]$  GeV, with a rescale factor of 3, 1 and 0.3, respectively.  $x_F$  is defined as  $x_F \equiv 2p_z / \sqrt{s}$ .

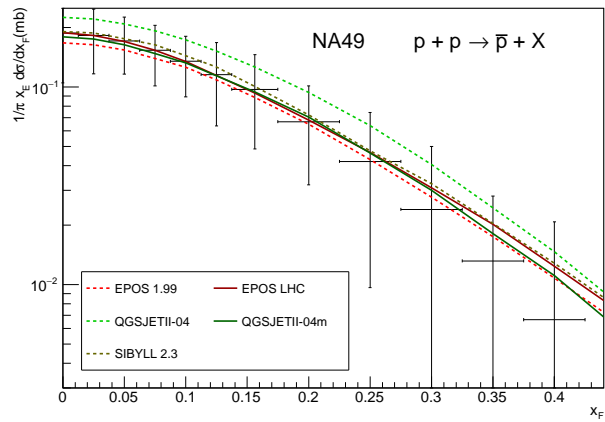


FIG. 2. The differential cross section of  $1/\pi x_E d\sigma/dx_F$  for the  $p + p \rightarrow \bar{p} + X$ .  $x_E$  is defined as  $x_E \equiv 2E_{\bar{p}}/\sqrt{s}$  in the center-of-mass system.

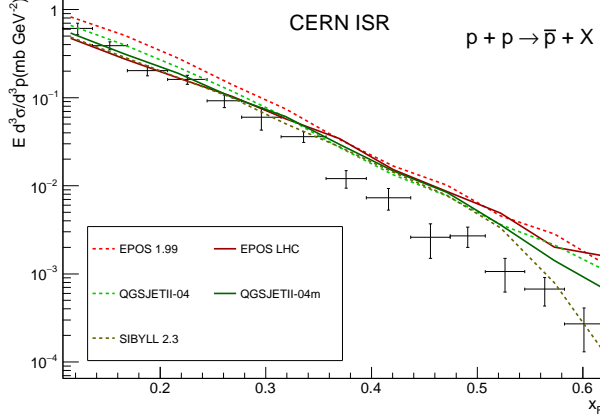


FIG. 3. The differential cross section of  $E d^3 \sigma / d^3 p$  for the  $p + p \rightarrow \bar{p} + X$  process compared with the CERN ISR experiment [59] with  $\sqrt{s} = 53 \text{ GeV}$ .

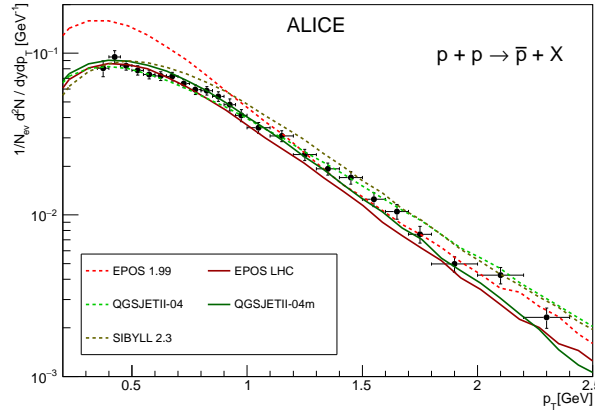


FIG. 4. The antiproton spectrum  $1/N d^2 N / dy dp$  for the  $p + p \rightarrow \bar{p} + X$  process as a function of the transverse momentum  $p_T$  in the center-of-mass system with  $\sqrt{s} = 900 \text{ GeV}$ . The rapidity  $y$  is cut with the condition  $|y| < 0.5$ . Also shown are the data from the ALICE experiment [51].

three representative ranges of  $p_T$  standing for the cases of low, medium and high  $p_T$ . As can be seen that all the models reproduce the cross section integrated over  $p_T$  well, but only QGSJET II-04m, EPOS LHC and SIBYLL could fit the differential cross section for the specified  $p_T$ .

For a higher energy region, we compare the model prediction with the data from the CERN ISR experiment [59] with the center-of-mass energy of  $\sqrt{s} = 53 \text{ GeV}$ . Such energy is relevant to the secondary antiprotons with energies of hundreds of GeV. In Fig. 3, we show the expectations of differential cross section for  $pp \rightarrow \bar{p}X$  and compare with the ISR data.



As can be seen that all the selected models reasonably reproduce the data in low  $x_F$  region, while slightly overestimate the antiproton in the high  $x_F$  region.

Finally, we compare the expectations with the measurement of the ALICE experiment at  $\sqrt{s} = 900\text{GeV}$ [51]. The antiprotons are for the rapidity  $|y| < 0.5$ . We find that all the selected hadronic models could give a good fit to the ALICE results except EPOS 1.99. Thus we conclude that the EPOS LHC and QGSJET II-04m models are suitable to predict the CR antiproton as they can interpret all the accelerator antiproton data well. Note that the center-of-mass energy 900GeV corresponding to a CR proton energy of 430TeV is far beyond the energy region relevant to the AMS-02 antiproton data. Therefore the EPOS 1.99 model is also adopted to calculate the CR antiproton flux, as it can interpret the low energy accelerator data well.

#### IV. ASTROPHYSICAL PREDICTION FOR THE $\bar{p}/p$ RATIO

In this section, we calculate the secondary antiproton flux generated by CRs when they propagate in the Galaxy, and study the uncertainties from the propagation and hadronic interaction models.

We use the numerical tool GALPROP [15, 20] to solve the propagation equation. The propagation parameters are determined by fitting the B/C and  $^{10}\text{Be}/^9\text{Be}$  data. In order to improve the fitting efficiency, the MCMC method is employed to derive the posterior probability distributions of propagation parameters. By fitting the B/C ratio data from AMS-02 [61] and ACE [62], and the  $^{10}\text{Be}/^9\text{Be}$  ratio data [63–71], we obtain the mean values and  $1\sigma$  errors of propagation parameters for the three propagation models, as shown in Table I. Here the proton injection spectrum is determined by fitting the AMS-02 [61] and CREAM [72] proton data. The proton spectrum hardening at  $\sim 200$  GeV can enhance the  $\bar{p}/p$  ratio at the high energy end.

In Fig. 5 we illustrate the  $\bar{p}/p$  ratio in the DR propagation model for different hadronic interaction models. The QGSJET II-04 overestimates the low energy antiprotons. This is not surprising since it does not reproduce the low energy accelerator data well as shown in Fig. 1. The fitting is improved in the modified QGSJET II-04 [53]. The SYBILL underestimates the low energy antiprotons greatly. The reason is that SYBILL does not extend to the cases with the incoming particles energy below  $\sim 60\text{GeV}$ . We do not consider

TABLE I. Mean values and  $1\sigma$  uncertainties of the propagation parameters derived through fitting the data of B/C and  $^{10}\text{Be}/^9\text{Be}$  ratios in three propagation models.

|                                       | DR                | DR-2              | DC                |
|---------------------------------------|-------------------|-------------------|-------------------|
| $D_0$ ( $10^{28}$ cm $^2$ s $^{-1}$ ) | $6.58 \pm 1.27$   | $3.59 \pm 0.88$   | $1.95 \pm 0.50$   |
| $\delta$                              | $0.333 \pm 0.011$ | $0.423 \pm 0.017$ | $0.510 \pm 0.034$ |
| $R_0$ (GV)                            | 4                 | 4                 | $4.71 \pm 0.80$   |
| $v_A$ (km s $^{-1}$ )                 | $37.8 \pm 2.7$    | $22.6 \pm 3.1$    | /                 |
| $dV_c/dz$ (km s $^{-1}$ kpc $^{-1}$ ) | /                 | /                 | $4.2 \pm 3.2$     |
| $z_h$ (kpc)                           | $4.7 \pm 1.0$     | $3.5 \pm 0.8$     | $2.5 \pm 0.7$     |
| $\phi_{B/C}$ (MV)                     | $326 \pm 36$      | $334 \pm 37$      | $182 \pm 25$      |

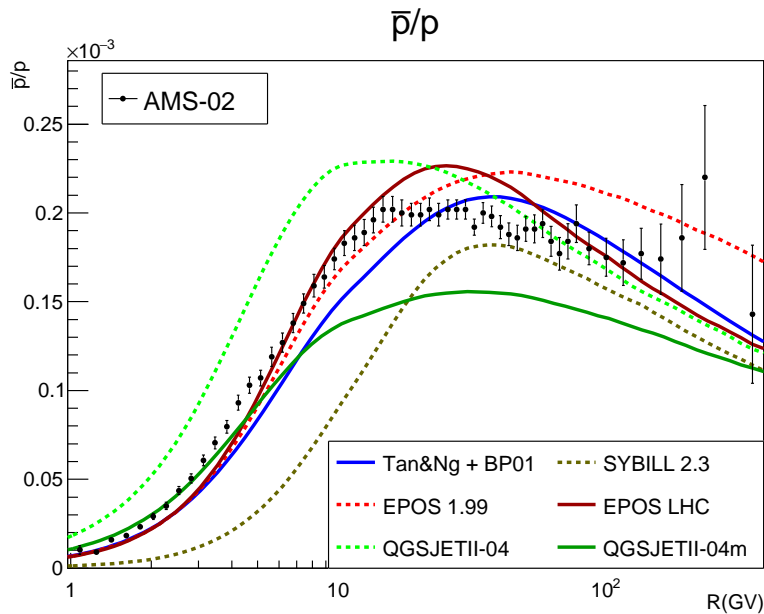


FIG. 5. The  $\bar{p}/p$  ratio expected from different hadronic models in the DR propagation model, in comparison with the AMS-02 measurement [4]. The propagation parameters used here give the best-fit to the B/C ratio, adopted from Ref. [25]:  $D_0 = 6.58 \times 10^{28}$  cm $^2$  s $^{-1}$ ,  $\delta = 0.33$ ,  $v_A = 37.8$  km s $^{-1}$ ,  $z_h = 4.7$  kpc,  $\nu_1 = 1.81$ ,  $\nu_2 = 2.40$ . The solar modulation potential is set to 800 MV.

the two interaction models later.

However, even the other four hadronic models provide diverse predictions. Note that the propagation parameters have been adjusted to fit the B/C data. Therefore the discrepancies

between the  $\bar{p}/p$  predictions and data may be due to the uncertainties in the nuclear reaction cross sections for  $C, O \rightarrow B$  or in the hadronic interactions for  $pp \rightarrow \bar{p}X$ . The uncertainties may also come from the heavy element interactions  $pA(AA) \rightarrow \bar{p}X$ . In order to include such effects, we introduce a free factor  $c_{\bar{p}}$  to slightly rescale the antiproton flux in order to fit the AMS-02 data. Therefore we present the prediction of  $\bar{p}$  flux and  $\bar{p}/p$  ratio, which is “calibrated” by the AMS-02 data, in the following, since the AMS-02 collaboration provides very precise measurements and well-controlled systematic errors.

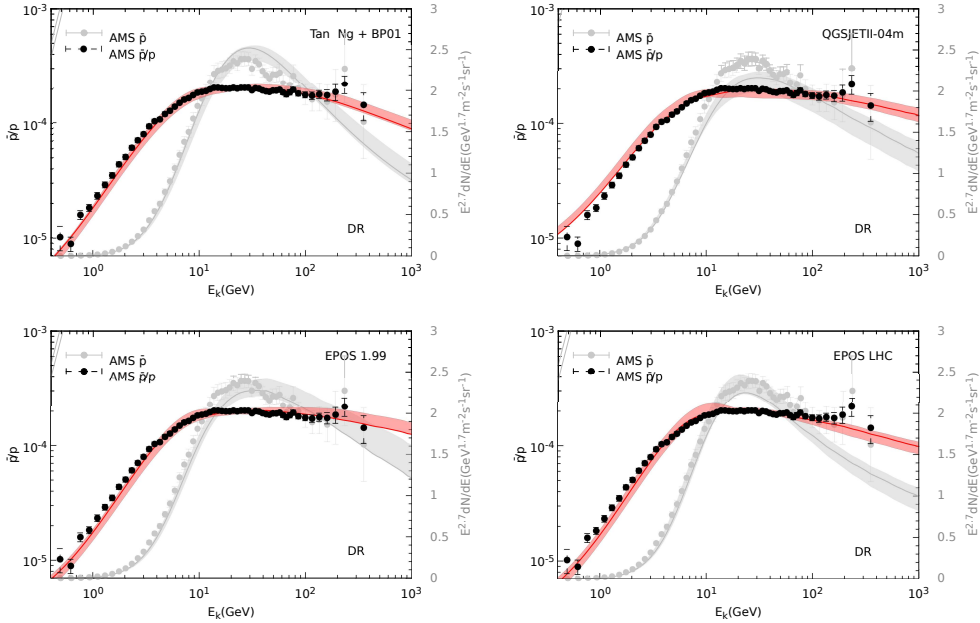


FIG. 6. The  $\bar{p}/p$  ratio (colored) and  $\bar{p}$  flux (gray) for different hadronic models in the DR model, comparing with the AMS-02 measurement [4]. The bands indicate the propagation uncertainty in 95% C.L., while the line is the best-fit case to the  $\bar{p}/p$  ratio. We have tuned the  $\bar{p}/p$  ratio with suitable rescaling and solar modulations to fit the data, and the  $\bar{p}$  flux prediction corresponds to this fit.

In Figs. 6, 7, and 8, we show the  $\bar{p}/p$  ratio and  $\bar{p}$  flux for four hadronic interaction models and three CR propagation models. To get these result, besides the scale factor  $c_{\bar{p}}$  we adopt a charge-dependent solar modulation potential to fit the AMS-02 data better. The colored bands of the  $\bar{p}/p$  ratio and the grey bands of  $\bar{p}$  flux represent the uncertainties of the corresponding propagation models with the propagation parameters varying within 95% confidence ranges. Note that the GALPROP default hadronic interaction model underestimates antiprotons at low energies compared with the AMS-02 data for the DR propagation

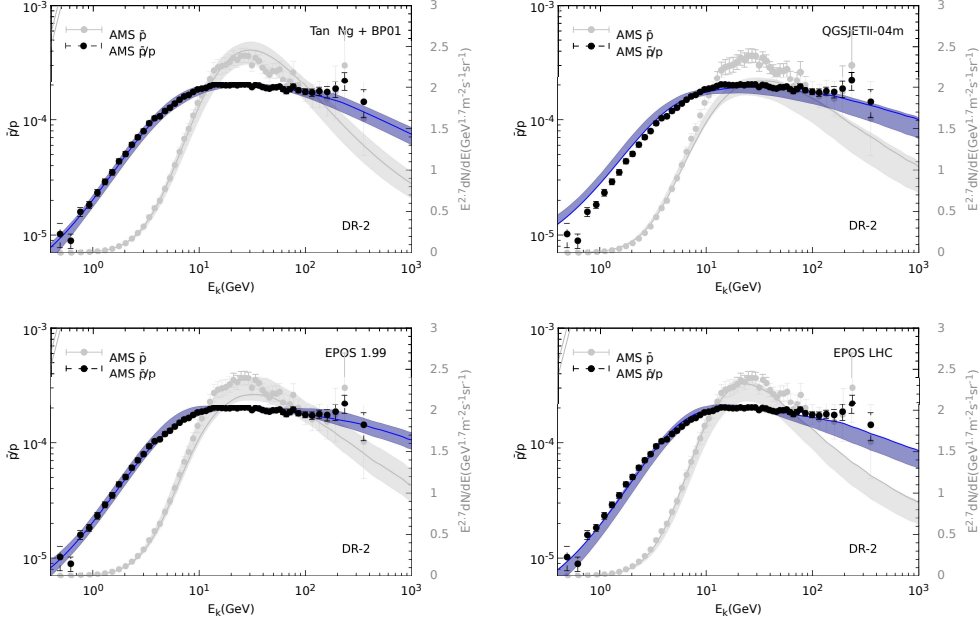


FIG. 7. The same as 6 but for the DR-2 model.

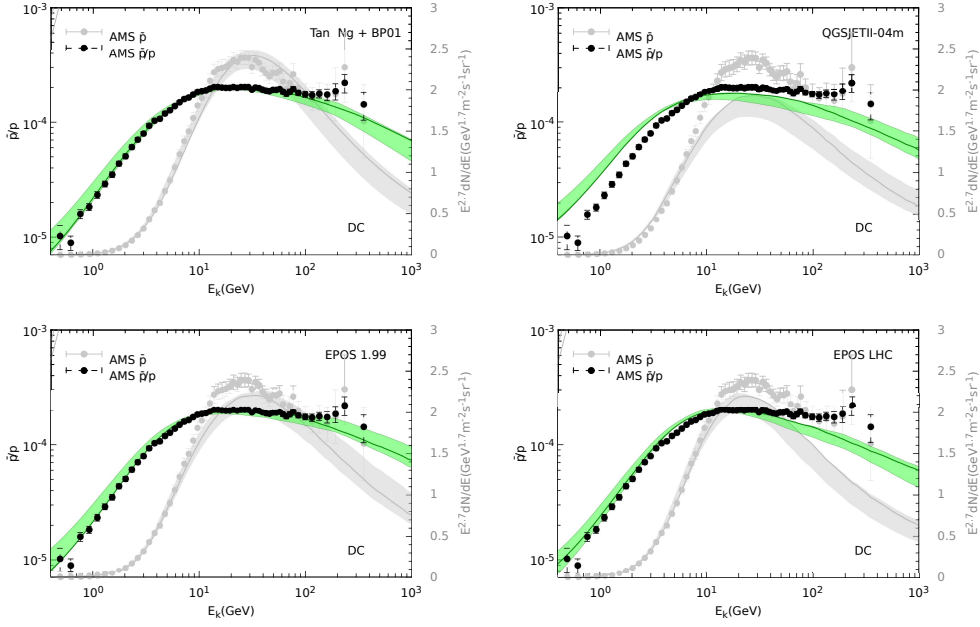


FIG. 8. The same as 6 but for the DC2 model.

model. Such an underproduction has been realized for a long time when studying the PAMELA [73, 74] and BESS [75] results [27, 76–78]. In order to solve this problem, the diffusion coefficient at low energies should be modified [77]. This is a motivation for introducing a factor  $\eta$  in the DR-2 model [29]. Here we note that this underproduction actually depends

on the hadronic interaction models too. On the contrary, the QGSJET-II04m model would overproduce antiprotons at low energies in the DR propagation model.

We find that the EPOS 1.99 model almost gives the best fit to the AMS-02 data in all three propagation models. It naturally predicts a flat  $\bar{p}/p$  ratio at the high energy end. On the other hand, the  $\bar{p}$  flux predicted by the QGSJET-II 04m model is not quite consistent with the AMS-02 data. The EPOS LHC model, which nearly best fit the accelerator data, seems to underestimate the  $\bar{p}/p$  ratio at the high energy end with obvious discrepancies compared to last several data points.

In Table II we show the parameters that can give best fit of the  $\bar{p}/p$  ratio to the AMS-02 data for the different propagation and hadronic interaction models. The propagation parameters are within the 95% *C.L.* range fitting to B/C. Here  $\phi_p$  is the solar modulation potential for protons by fitting to the AMS-02 proton spectrum. The solar modulation potential value for antiproton  $\phi_{\bar{p}}$  is only slightly different from  $\phi_p$ . We notice that the rescale factor  $c_{\bar{p}}$  is near 1 within 20%. It can be seen that the EPOS 1.99 and the GALPROP default models can well fit the AMS-02 data with small  $\chi^2$  values. EPOS LHC also provides an acceptable fit to the data, while QGSJET II-04m tends to give a large  $\chi^2$ .

## V. IMPLICATIONS FOR DARK MATTER ANNIHILATION

As shown in the previous section, the theoretical prediction of the antiproton flux has quite large uncertainties. In some cases the prediction fit the AMS-02 data very well, which can give a strong constraint on the dark matter annihilation. However, in some cases, there are discrepancies between the prediction and the data, which may indicate a contribution from dark matter. We discuss the implications on DM annihilation according to the AMS-02 antiproton result in this section.

We use the results of PPC 4 DM ID [79] including the electroweak corrections [80] to calculate DM annihilation. The DM density distribution is assumed to be the Navarro-Frenk-White (NFW) profile [81] with the local density of  $0.3 \text{ GeV cm}^{-3}$ . In Figs. 9, 10, and 11, we set upper bounds on the DM annihilation cross sections in the  $b\bar{b}$  and  $W^+W^-$  channels at 95% C.L. by using the AMS-02  $\bar{p}/p$  result. Note that if the discrepancies between the predicted  $\bar{p}/p$  ratio and the AMS-02 data at the high energy end are taken seriously, there may be room for DM signals at high energies. Therefore, we also attempt to introduce

|                  | Tan & Ng + BP01 |         |         | EPOS LHC |         |         | EPOS 1.99 |         |         | QGSJETII-04m |        |         |
|------------------|-----------------|---------|---------|----------|---------|---------|-----------|---------|---------|--------------|--------|---------|
|                  | DR              | DR2     | DC      | DR       | DR2     | DC      | DR        | DR2     | DC      | DR           | DR2    | DC      |
| $c_{\bar{p}}$    | 1.15            | 1.05    | 0.99    | 0.899    | 0.959   | 0.76    | 0.923     | 0.853   | 0.836   | 1.22         | 1.2    | 1.04    |
| $\phi_{\bar{p}}$ | 0.429           | 0.69    | 0.773   | 0.468    | 0.928   | 0.809   | 0.462     | 0.592   | 0.823   | 0.58         | 0.843  | 0.823   |
| $\chi^2$         | 77.9/57         | 38.9/57 | 51.6/57 | 131/57   | 78.1/57 | 300/57  | 119/57    | 28.9/57 | 57.3/57 | 119/57       | 298/57 | 1419/57 |
| $\phi_p$         | 0.515           | 0.745   | 0.644   | 0.562    | 0.773   | 0.674   | 0.554     | 0.71    | 0.686   | 0.483        | 0.703  | 0.686   |
| $D_0$            | 7.76            | 2.87    | 1.4     | 6.68     | 2.79    | 2.39    | 6.05      | 2.91    | 1.8     | 7.19         | 4.34   | 1.8     |
| $\delta^a$       | 0.337           | 0.433   | 0/0.453 | 0.338    | 0.42    | 0/0.478 | 0.335     | 0.418   | 0/0.523 | 0.324        | 0.39   | 0/0.523 |
| $R_0$            | —               | —       | 3.87    | —        | —       | 3.62    | —         | —       | 5.78    | —            | —      | 5.78    |
| L                | 5.46            | 2.8     | 1.69    | 4.92     | 2.78    | 3.13    | 4.38      | 2.86    | 2.17    | 4.79         | 3.92   | 2.17    |
| $v_A$            | 41.3            | 22.2    | —       | 34.4     | 18.9    | —       | 33.9      | 19.5    | —       | 42.5         | 24.4   | —       |
| $dV_c/dz$        | —               | —       | 0.326   | —        | —       | 2.97    | —         | —       | 2.68    | —            | —      | 2.68    |

<sup>a</sup> The  $\delta$  would be 0 for  $R < R_0$  in the DC case

TABLE II. The values of parameters for the best fit to data in different scenarios.

a DM signal to improve the fitting quality, and show corresponding regions of the parameter space in Figs. 9, 10, and 11.

Fig. 9 shows the upper limits on the DM annihilation cross sections for the  $b\bar{b}$  and  $W^+W^-$  final states for the QGSJET II-04m model. Here we only give the constraint in the DR propagation model, since in the other two propagation models the secondary  $\bar{p}/p$  predictions can not fit the data to derive a reasonable bound. The red bands represent the uncertainties from the propagation model. For comparison, the limits from the Fermi-LAT gamma-ray observation of dwarf galaxies are also shown in the plots. We can see that the constraints from the AMS-02  $\bar{p}/p$  result are more stringent than the Fermi-LAT constraints. We also find a small parameter region located around 200 GeV, where a DM annihilation signal would improve the fitting quality.

In Fig. 10 we set constraints for the EPOS-LHC model. The constraints are worse than the Fermi dwarf galaxy constraints, since the EPOS LHC model generally predicts a slightly lower  $\bar{p}/p$  ratio than the data at the high energy end. Recalling that the EPOS LHC model fits the accelerator data well, such discrepancies should be taken seriously. In order

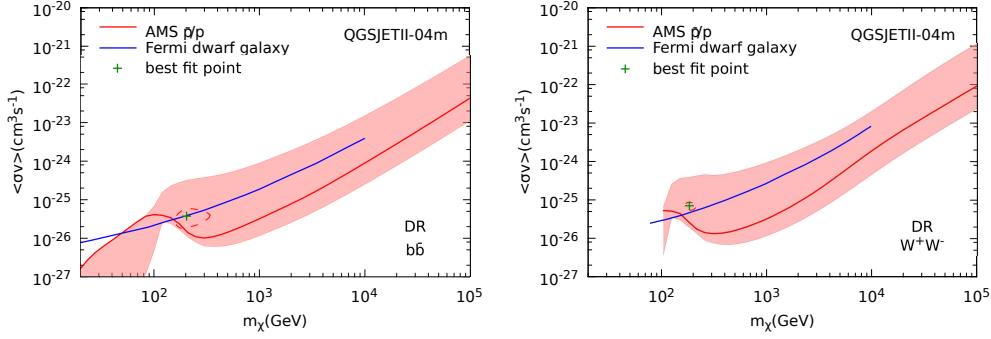


FIG. 9. The 95% upper limits on the dark matter annihilation rate  $\langle\sigma v\rangle$  derived from the AMS-02  $\bar{p}/p$  ratio for QGSJET II-04m with the DR propagation model. The left panel is for the  $\bar{b}b$  channel, and the right panel is for the  $W^+W^-$  channel. The red bands indicate the propagation uncertainty in 95% C.L., while the red line is corresponding to the case that fit to the  $\bar{p}/p$  best. For comparison, we also show the upper limits from the Fermi-LAT observation of dwarf galaxies [82] as the blue lines. The contour denotes a DM signal in the 68% confidence region favored by the AMS-02  $\bar{p}/p$  ratio data in the  $m_\chi - \langle\sigma v\rangle$  plane.

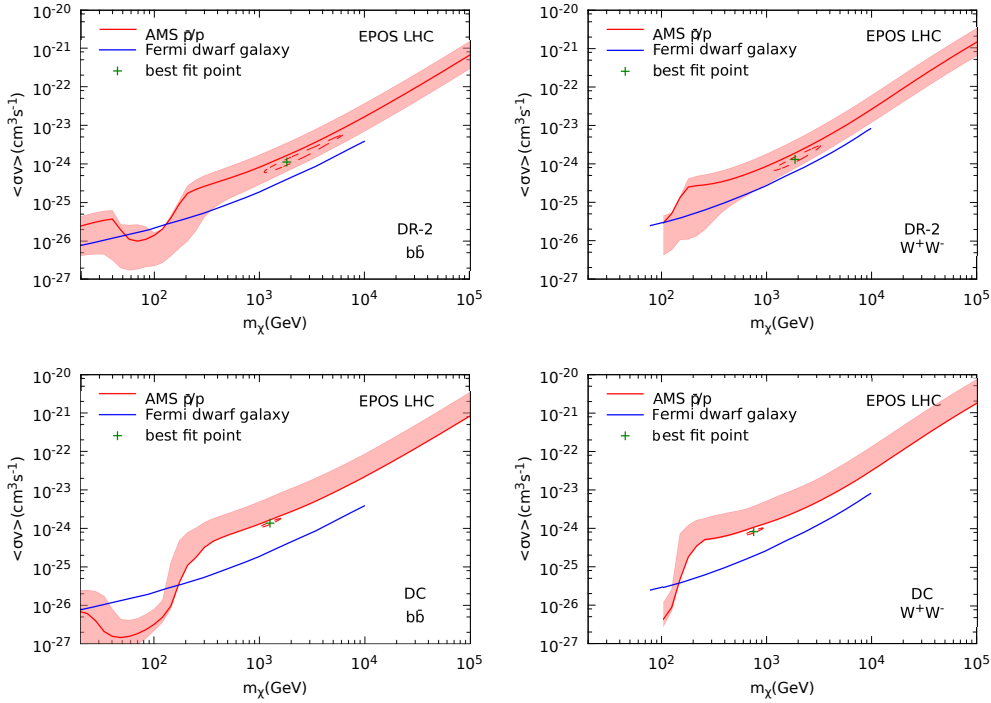


FIG. 10. The same as Fig. 9, but for EPOS LHC interaction model with the DR-2 and DC propagation models.

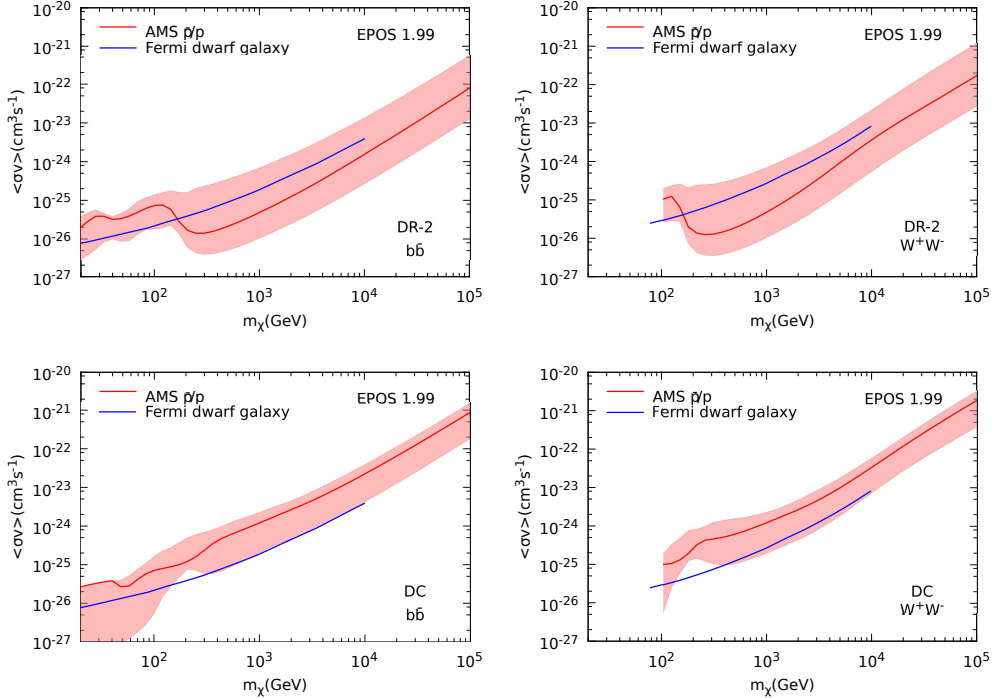


FIG. 11. The same as Fig. 9, but for EPOS 1.99 interaction model with the DR-2 and DC propagation models.

to improve the fit, a DM signal with a mass of  $\sim \text{TeV}$  can be introduced. However, the corresponding DM annihilation signal seems to be excluded by Fermi. Here we mention that such a contradiction may be evaded, if a velocity-dependent DM annihilation cross section is introduced [83].

We give the constraints for the EPOS 1.99 model in Fig. 11. As the EPOS 1.99 model fits the AMS-02 antiproton data best, it sets very stringent constraints on the DM annihilation cross section.

## VI. CONCLUSIONS

In this work we recalculate the astrophysical CR  $\bar{p}/p$  ratio and  $\bar{p}$  flux, and compare them with the latest AMS-02 results. We investigate the uncertainties from the propagation models and the hadronic interaction models.

We consider the DR, DR-2, and DC propagation models, where the propagation parameters are determined by fitting the B/C and  $^{10}\text{Be}/^9\text{Be}$  data with a MCMC algorithm. All



these models can provide a very good fit to the B/C data.

We note that the uncertainties from propagation and hadronic interaction may interplay with each other. For example, it has been recognized that the DR propagation model may underestimate the  $\bar{p}$  flux at low energies by GALPROP [27, 76–78]. However, we find that the  $\bar{p}$  flux is even overproduced at low energies if the QGSJET II-04 model is adopted. For the DR-2 and DC propagation models, the predictions given by QGSJET II-04m seem not consistent with the AMS-02  $\bar{p}$  data, while other three interaction models can fit the data quite well.

We further derive the upper bound on the DM annihilation cross section from the AMS-02  $\bar{p}/p$  data. It is found that in most cases the bound can be stronger than the constraint from Fermi observation of the dwarf galaxies.

Among these interaction models, the EPOS LHC model can fit the NA49 and LHC data very well. However, this model predicts a slightly lower  $\bar{p}/p$  ratio than the AMS-02 data at the high energy end. If such a discrepancy is taken seriously, a  $\sim$  TeV DM annihilation signal is necessary to fit the AMS-02 data.

## ACKNOWLEDGMENTS

We thank Qiang Yuan, Sergey Ostapchenko for helpful discussions. We appreciate Tanguy Peirog, Colin Baus, and Ralf Ulrich for the CRMC interface to access the hadronic models. This work is supported by the National Natural Science Foundation of China under Grants No. 11475189, 11475191, by the 973 Program of China under Grant No. 2013CB837000, and by the National Key Program for Research and Development (No. 2016YFA0400200).

- 
- [1] “Ams-02,” <http://www.ams02.org/>.
  - [2] “Welcome to pamelamission official website,” <http://pamelamission.roma2.infn.it/>.
  - [3] “Fermi large area telescope,” <https://www-glast.stanford.edu/>.
  - [4] M. Aguilar *et al.* (AMS), Phys. Rev. Lett. **117**, 091103 (2016).
  - [5] G. Giesen, M. Boudaud, Y. Genolini, V. Poulin, M. Cirelli, *et al.*, (2015), arXiv:1504.04276 [astro-ph.HE].

- [6] S.-J. Lin, X.-J. Bi, P.-F. Yin, and Z.-H. Yu, (2015), arXiv:1504.07230 [hep-ph].
- [7] H.-B. Jin, Y.-L. Wu, and Y.-F. Zhou (2015) arXiv:1508.06844 [hep-ph].
- [8] C.-H. Chen, C.-W. Chiang, and T. Nomura, (2015), arXiv:1504.07848 [hep-ph].
- [9] M. Ibe, S. Matsumoto, S. Shirai, and T. T. Yanagida, (2015), arXiv:1504.05554 [hep-ph].
- [10] K. Hamaguchi, T. Moroi, and K. Nakayama, (2015), arXiv:1504.05937 [hep-ph].
- [11] K. Kohri, K. Ioka, Y. Fujita, and R. Yamazaki, (2015), arXiv:1505.01236 [astro-ph.HE].
- [12] R. Kappl, A. Reinert, and M. W. Winkler, (2015), arXiv:1506.04145 [astro-ph.HE].
- [13] B.-Q. Lu and H.-S. Zong, (2015), arXiv:1510.04032 [astro-ph.HE].
- [14] J. Feng, N. Tomassetti, and A. Oliva, (2016), arXiv:1610.06182 [astro-ph.HE].
- [15] A. Strong and I. Moskalenko, *Astrophys.J.* **509**, 212 (1998), arXiv:astro-ph/9807150 [astro-ph].
- [16] T. K. Gaisser, *Cambridge and New York, Cambridge University Press, 1990, 292 p.* (1990).
- [17] G. Di Bernardo, C. Evoli, D. Gaggero, D. Grasso, and L. Maccione, *Astropart. Phys.* **34**, 274 (2010), arXiv:0909.4548 [astro-ph.HE].
- [18] D. Maurin, F. Donato, R. Taillet, and P. Salati, *Astrophys. J.* **555**, 585 (2001), arXiv:astro-ph/0101231 [astro-ph].
- [19] L. J. Gleeson and W. I. Axford, *Astrophys. J.* **154**, 1011 (1968).
- [20] I. V. Moskalenko and A. W. Strong, *Astrophys. J.* **493**, 694 (1998), arXiv:astro-ph/9710124 [astro-ph].
- [21] A. Lewis and S. Bridle, *Phys.Rev.* **D66**, 103511 (2002), arXiv:astro-ph/0205436 [astro-ph].
- [22] J. Liu, Q. Yuan, X. Bi, H. Li, and X. Zhang, *Phys. Rev.* **D81**, 023516 (2010), arXiv:0906.3858 [astro-ph.CO].
- [23] J. Liu, Q. Yuan, X.-J. Bi, H. Li, and X. Zhang, *Phys. Rev.* **D85**, 043507 (2012), arXiv:1106.3882 [astro-ph.CO].
- [24] Q. Yuan, X.-J. Bi, G.-M. Chen, Y.-Q. Guo, S.-J. Lin, *et al.*, *Astropart.Phys.* **60**, 1 (2015), arXiv:1304.1482 [astro-ph.HE].
- [25] S.-J. Lin, Q. Yuan, and X.-J. Bi, *Phys. Rev.* **D91**, 063508 (2015), arXiv:1409.6248 [astro-ph.HE].
- [26] A. W. Strong, I. V. Moskalenko, and V. S. Ptuskin, *Ann.Rev.Nucl.Part.Sci.* **57**, 285 (2007), arXiv:astro-ph/0701517 [astro-ph].
- [27] R. Trotta, G. Johannesson, I. Moskalenko, T. Porter, R. R. de Austri, *et al.*,

- Astrophys.J. **729**, 106 (2011), arXiv:1011.0037 [astro-ph.HE].
- [28] D. Maurin, A. Putze, and L. Derome, *Astron.Astrophys.* **516**, A67 (2010), arXiv:1001.0553 [astro-ph.HE].
- [29] G. Di Bernardo, C. Evoli, D. Gaggero, D. Grasso, L. Maccione, and M. N. Mazziotta, *Astropart. Phys.* **34**, 528 (2011), arXiv:1010.0174 [astro-ph.HE].
- [30] E. S. Seo and V. S. Ptuskin, *Astrophys. J.* **431**, 705 (1994).
- [31] A. Putze, L. Derome, and D. Maurin, *Astron. Astrophys.* **516**, A66 (2010), arXiv:1001.0551 [astro-ph.HE].
- [32] G. Corcella, I. G. Knowles, G. Marchesini, S. Moretti, K. Odagiri, P. Richardson, M. H. Seymour, and B. R. Webber, *JHEP* **01**, 010 (2001), arXiv:hep-ph/0011363 [hep-ph].
- [33] T. Sjostrand, S. Mrenna, and P. Z. Skands, *JHEP* **05**, 026 (2006), arXiv:hep-ph/0603175 [hep-ph].
- [34] T. Gleisberg, S. Hoeche, F. Krauss, M. Schonherr, S. Schumann, F. Siegert, and J. Winter, *JHEP* **02**, 007 (2009), arXiv:0811.4622 [hep-ph].
- [35] N. N. Kalmykov, S. S. Ostapchenko, and A. I. Pavlov, *Proceedings, 9th International Symposium on Very High Energy Cosmic Ray Interactions (ISVHECRI 1996)*, *Nucl. Phys. Proc. Suppl.* **52**, 17 (1997).
- [36] S. Ostapchenko, *Proceedings, 13th International Symposium on Very High-Energy Cosmic Ray Interactions (ISVHECRI 2004)*, *Nucl. Phys. Proc. Suppl.* **151**, 143 (2006), arXiv:hep-ph/0412332 [hep-ph].
- [37] S. Ostapchenko, *Phys. Rev.* **D74**, 014026 (2006), arXiv:hep-ph/0505259 [hep-ph].
- [38] J. Engel, T. K. Gaisser, T. Stanev, and P. Lipari, *Phys. Rev.* **D46**, 5013 (1992).
- [39] R. S. Fletcher, T. K. Gaisser, P. Lipari, and T. Stanev, *Phys. Rev.* **D50**, 5710 (1994).
- [40] E.-J. Ahn, R. Engel, T. K. Gaisser, P. Lipari, and T. Stanev, *Phys. Rev.* **D80**, 094003 (2009), arXiv:0906.4113 [hep-ph].
- [41] R. Engel, *Z. Phys.* **C66**, 203 (1995).
- [42] R. Engel and J. Ranft, *Phys. Rev.* **D54**, 4244 (1996), arXiv:hep-ph/9509373 [hep-ph].
- [43] R. Engel, J. Ranft, and S. Roesler, *Phys. Rev.* **D52**, 1459 (1995), arXiv:hep-ph/9502319 [hep-ph].
- [44] F. W. Bopp, J. Ranft, R. Engel, and S. Roesler, *Phys. Rev.* **C77**, 014904 (2008), arXiv:hep-ph/0505035 [hep-ph].

- [45] K. Werner, F.-M. Liu, and T. Pierog, Phys. Rev. **C74**, 044902 (2006), arXiv:hep-ph/0506232 [hep-ph].
- [46] T. Pierog, I. Karpenko, J. M. Katzy, E. Yatsenko, and K. Werner, Phys. Rev. **C92**, 034906 (2015), arXiv:1306.0121 [hep-ph].
- [47] S. Ostapchenko, Phys. Rev. **D83**, 014018 (2011), arXiv:1010.1869 [hep-ph].
- [48] S. Chatrchyan *et al.* (CMS), Eur. Phys. J. **C72**, 2164 (2012), arXiv:1207.4724 [hep-ex].
- [49] T. Csrg *et al.* (TOTEM), *Proceedings, 41st International Symposium on Multiparticle Dynamics (ISMD 2011): Miyajima, Hiroshima, Japan, September 26-30, 2011*, Prog. Theor. Phys. Suppl. **193**, 180 (2012), arXiv:1204.5689 [hep-ex].
- [50] K. Aamodt *et al.* (ALICE), Eur. Phys. J. **C68**, 345 (2010), arXiv:1004.3514 [hep-ex].
- [51] K. Aamodt *et al.* (ALICE), Eur. Phys. J. **C71**, 1655 (2011), arXiv:1101.4110 [hep-ex].
- [52] G. Aad *et al.* (ATLAS), New J. Phys. **13**, 053033 (2011), arXiv:1012.5104 [hep-ex].
- [53] M. Kachelriess, I. V. Moskalenko, and S. S. Ostapchenko, (2015), arXiv:1502.04158 [astro-ph.HE].
- [54] T. Pierog and K. Werner, *Proceedings, 15th International Symposium on Very High Energy Cosmic Ray Interactions (ISVHECRI 2008): Paris, France, September 1-6, 2008*, Nucl. Phys. Proc. Suppl. **196**, 102 (2009), arXiv:0905.1198 [hep-ph].
- [55] K. Grebieszko (NA61, NA49), *Nuclear physics and the road to FAIR. Proceedings, 31st Mazurian Lakes Conference on Physics, Piaski, Poland, August 30-September 6, 2009*, Acta Phys. Polon. **B41**, 427 (2010), arXiv:0911.1902 [nucl-ex].
- [56] I. V. Moskalenko, A. W. Strong, and O. Reimer, Astron. Astrophys. **338**, L75 (1998), arXiv:astro-ph/9808084 [astro-ph].
- [57] L. C. Tan and L. K. Ng, Journal of Physics G Nuclear Physics **9**, 1289 (1983).
- [58] T. Anticic *et al.* (NA49), Eur. Phys. J. **C65**, 9 (2010), arXiv:0904.2708 [hep-ex].
- [59] M. G. Albrow *et al.* (CHLM), Nucl. Phys. **B56**, 333 (1973).
- [60] B. Baatar *et al.* (NA49), Eur. Phys. J. **C73**, 2364 (2013), arXiv:1207.6520 [hep-ex].
- [61] A.-. Collaboration, *International Cosmic-Ray Conference*, (2013), <http://www.ams02.org/2013/07/newresults-from-ams-presented-at-icrc-2013/>.
- [62] AIP Conf. Proc. 528 (2000) 452 p (2000).
- [63] N. E. Yanasak, M. E. Wiedenbeck, R. A. Mewaldt, A. J. Davis, A. C. Cummings, J. S. George, R. A. Leske, E. C. Stone, E. R. Christian, T. T. von Rosenvinge, W. R. Binns, P. L. Hink,

- and M. H. Israel, *Astrophys. J.* **563**, 768 (2001).
- [64] F. A. Hagen, A. J. Fisher, and J. F. Ormes, *Astrophys. J.* **212**, 262 (1977).
- [65] A. Buffington, C. D. Orth, and T. S. Mast, *Astrophys. J.* **226**, 355 (1978).
- [66] W. R. Webber and J. Kish, *International Cosmic Ray Conference* **1**, 389 (1979).
- [67] M. Garcia-Munoz, J. A. Simpson, and J. P. Wefel, *International Cosmic Ray Conference* **2**, 72 (1981).
- [68] J. A. Simpson and M. Garcia-Munoz, *Space Sci. Rev.* **46**, 205 (1988).
- [69] T. Hams *et al.*, *Astrophys. J.* **611**, 892 (2004).
- [70] J. J. Connell, *Astrophys. J. Lett.* **501**, L59 (1998).
- [71] A. Lukasiak, *International Cosmic Ray Conference* **3**, 41 (1999).
- [72] H. Ahn, P. Allison, M. Bagliesi, J. Beatty, G. Bigongiari, *et al.*, *Astrophys. J.* **714**, L89 (2010), arXiv:1004.1123 [astro-ph.HE].
- [73] O. Adriani *et al.*, *Phys. Rev. Lett.* **102**, 051101 (2009), arXiv:0810.4994 [astro-ph].
- [74] O. Adriani *et al.* (PAMELA), *Phys. Rev. Lett.* **105**, 121101 (2010), arXiv:1007.0821 [astro-ph.HE].
- [75] S. Orito *et al.* (BESS), *Phys. Rev. Lett.* **84**, 1078 (2000), arXiv:astro-ph/9906426 [astro-ph].
- [76] C. Evoli, I. Cholis, D. Grasso, L. Maccione, and P. Ullio, *Phys. Rev.* **D85**, 123511 (2012), arXiv:1108.0664 [astro-ph.HE].
- [77] I. V. Moskalenko, A. W. Strong, J. F. Ormes, and M. S. Potgieter, *Astrophys. J.* **565**, 280 (2002), arXiv:astro-ph/0106567 [astro-ph].
- [78] D. Hooper, T. Linden, and P. Mertsch, *JCAP* **1503**, 021 (2015), arXiv:1410.1527 [astro-ph.HE].
- [79] M. Cirelli, G. Corcella, A. Hektor, G. Hutsi, M. Kadastik, *et al.*, *JCAP* **1103**, 051 (2011), arXiv:1012.4515 [hep-ph].
- [80] P. Ciafaloni, D. Comelli, A. Riotto, F. Sala, A. Strumia, *et al.*, *JCAP* **1103**, 019 (2011), arXiv:1009.0224 [hep-ph].
- [81] J. F. Navarro, C. S. Frenk, and S. D. White, *Astrophys. J.* **490**, 493 (1997), arXiv:astro-ph/9611107 [astro-ph].
- [82] M. Ackermann *et al.* (Fermi-LAT), (2015), arXiv:1503.02641 [astro-ph.HE].
- [83] Y. Zhao, X.-J. Bi, H.-Y. Jia, P.-F. Yin, and F.-R. Zhu, *Phys. Rev.* **D93**, 083513 (2016), arXiv:1601.02181 [astro-ph.HE].